Journal of Nuclear Materials 385 (2009) 351–357

Contents lists available at ScienceDirect

Journal of Nuclear Materials

journal homepage: www.elsevier.com/locate/jnucmat

A molecular dynamics study of radiation induced diffusion in uranium dioxide

G. Martin [a,*], S. Maillard [a], L. Van Brutzel [b], P. Garcia [a], B. Dorado [a], C. Valot [a]

[a] CEA, DEN, DEC, Cadarache, 13108 Saint-Paul-lez-Durance, France
[b] CEA, DEN, DPC, Saclay, 91191 Gif-sur-Yvette, France

ARTICLE INFO

PACS:
31.15.Xv
61.80.Az
66.30.hd

ABSTRACT

The nuclear oxide fuels are submitted 'in-pile' to strong structural and chemical modifications due to the fissions and temperature. The diffusion of species is notably the result of a thermal activation and of radiation induced diffusion. This study proposes to estimate to what extent the radiation induced diffusion contributes to the diffusion of lattice atoms in UO_2. Irradiations are simulated using molecular dynamics simulation by displacement cascades induced by uranium primary knock-on atoms between 1 and 80 keV. As atoms are easier to displace when their vibration amplitude increases, the temperature range which have been investigated is 300–1400 K. Cascade overlaps were also simulated. The material is shown to melt at the end of cascades, yielding a reduced threshold energy displacement. The nuclear contribution to the radiation induced diffusion is compared to thermally activated diffusion under in-reactor and long-term storage conditions.

1. Introduction

During reactor operation, fission fragments generated within the oxide fuel lose their kinetic energy through two different processes. At high energy, the fission fragment energy loss essentially originates from inelastic interactions such as electronic excitation of atoms in the fuel matrix, which could result in the displacement of atoms located along the ion trajectory. At lower energies, energy loss occurs through ballistic collisions between atoms. This second process of energy loss, which is also relevant under long-term storage conditions, leads to the formation of displacement cascades, liable to induce long range atomic migration. The electronic and nuclear contributions to migration processes associated with the irradiation are usually referred to radiation induced diffusion (RID). Since this phenomenon is a key ingredient in all fuel performance applications, it is essential, if one aims at developing predictive approaches, that atomistic models be used to ascertain what physical processes contribute to it and to what extent.

Basic experimental data demonstrating RID in uranium dioxide is hard to come by. Höh and Matzke [1] estimated the cation RID coefficient through a set of in-pile trace diffusion experiments at roughly 10^{-20} m^2 s^{-1} for fission densities of about 10^{19} m^{-3} s^{-1}. Later RID was shown to be completely a thermal below 1375 K. Turnbull et al. [2] studied the in-pile release of volatile fission products, rare gases in particular. They deduced from their experiments a thermal diffusion coefficients very similar to those obtained by Höh and Matzke (between 1×10^{-21} and 5×10^{-21} m^2 s^{-1} for xenon at similar fission rates). Hocking et al. [3] have more recently attempted to characterise RID of iodine through experiments involving iodine in implanted polycrystalline sintered samples irradiated with energetic ions simulating the effects of fission fragments. Which physical phenomena actually cause the observed mobility of atoms in-pile (displacement cascades, electronic excitations of slowing fission fragments, temperature assisted migration in the presence of enhanced quantities of defects...) still remains unclear. The aim of this paper is to help shed light on the matter using MD models.

Molecular dynamics (MD) tools can indeed be used to estimate irradiation induced phenomena [4]. In this paper classical molecular dynamics simulations are applied using the interatomic potential developed by Morelon et al. [5] in an attempt to estimate ballistic mixing effects and their possible temperature dependence. Collision cascades were simulated at varying temperatures from 300 to 1400 K, a range which covers the temperatures relevant under normal operating conditions and under long-term storage conditions. Because of the computational resources required for such calculations, the energy of the projectile, a uranium primary knock-on atom (PKA), is limited to several tens of keV. Simulations were therefore performed with various incident projectile energies in order to enable the extrapolation of results for more realistic PKA energies.

2. Calculation conditions

A UO_2 infinite matrix with periodic boundary conditions is simulated by molecular dynamics using the empirical interatomic

* Corresponding author. Tel.: +33 4 42 25 27 31; fax: +33 4 42 25 13 37.
E-mail address: guillaume.martin@cea.fr (G. Martin).

0022-3115/$ - see front matter © 2008 Elsevier B.V. All rights reserved.
doi:10.1016/j.jnucmat.2008.12.010

potentials described in [5] based on a rigid ion model, with respective charges for oxygen anions and uranium cations of −1.61362 and of +3.22725. The U–U interaction is a pure repulsive Coulomb interaction. The analytical form of the U–O potential is composed of a Born–Mayer–Huggins (BMH) repulsive term, and of an attractive part composed of a Van Der Waals term and a coulombic term. The repulsive O–O potential is unconventional and is defined by intervals: short distance interactions are simulated by a BMH potential, long range interactions by a Van Der Waals term and medium range interactions by successive fifth-degree and third-degree polynomials.

This potential provides results relative to point defects which are in good agreement with experimental data [6]. It is also consistent with other experimental data relative to physical properties such as the thermal expansion coefficient, heat capacity [7] or oxygen diffusion coefficient [8,9]. Molecular dynamics simulations of displacement cascade overlaps have moreover shown the fluorite structure not to be susceptible to amorphisation under irradiation, which corroborates experimental observations.

The BMH like potentials give a good description of the interaction between two ions at equilibrium but interatomic distances can be much less than their equilibrium distance during a displacement cascade event. For interatomic distances typically <0.16 nm, a Ziegler–Biersack–Littmark (ZBL) potential is therefore used, of which the continuity with the BMH potential is ensured by a fifth-degree polynomial. The forces and their first derivative are continuous at the transition point.

The initial cubic box that contains 25^3–68^3 perfect UO_2 unit cells is first relaxed under constant number of atoms, pressure and temperature (NPT conditions), the temperature of the box being regulated by a Nosé chain [10]. The second step consists in accelerating a single uranium ion at constant volume and a conservative energy (NV″E″ conditions) inside the core of the simulation box which has reached equilibrium after the first run to simulate a primary knock-on atom (PKA). A thermostat is applied at the box sides by rescaling the velocities of some atoms within the first atomic cell (over 0.3 nm). Cascades were performed with uranium PKA from 1 to 80 keV at temperatures ranging between 300 and 1400 K. Each MD simulation lasts ~25 ps divided into 50 000 time steps. The used variable-step algorithm, which enables the reduction of the computational time, is described in [11]. The cascade initiated at 80 keV has been presented previously [12]. Ten initial PKA directions were chosen to cover as different directions as possible: the angle between the normalised initial velocities and all equivalents towards the UO_2 crystal of any two PKA is at least 9°. Several calculations were performed for each set of conditions to provide a statistical approach to the modelling results, changing only the initial direction and location of the uranium PKA. Cascade overlaps were also simulated by starting cascade simulations from the final configuration of previous runs. Table 1 gathers the conditions of all simulations sets for different initial PKA energies and at different temperatures, each temperature corresponding to a specific equilibrium lattice parameter.

Table 1
Overview of the temperatures and uranium PKA energies which were used to simulate each simulation set of MD cascades in NV″E″ conditions.

Uranium PKA energy (keV)	Temperature (K)	Cascade overlaps	Number of cascades	Lattice parameter (nm)
80	300	–	1	0.5468
10	1400	2–6	15 (5 × 3)	0.56382
10	1400	–	9	0.56382
10	1100	–	9	0.5608
10	700	2–14	39 (13 × 3)	0.55635
10	700	–	9	0.55635
5	700	–	9	0.55635
2	700	–	9	0.55635
1	700	–	9	0.55635

3. Description of displacement cascades

3.1. Successive stages which describe a cascade

As described in [12], different successive phases occur during a displacement cascade. Fig. 1(a), which shows all atoms of the initial perfect UO_2 lattice in a plane perpendicular to the <1 1 0> direction at 700 K, reveals the empty octahedral interstitial sites which are aligned along this direction. Atoms which have been displaced by more than 0.15 nm appear in Fig. 1(b), (c) and (d) at different stages of a 10 keV cascade. First, within a few tenths of ps, a ballistic phase is created during which long range migration of atoms can occur. This phase leads to the formation of sub-cascade branches. During a second stage, the energy of the cascade is thermally dissipated and a molten volume appears which lasts a few ps. During this stage, an elastic wave similar to that described in [12] for an 80 keV PKA can be observed (see Fig. 1(c)) but not as clearly as in [12] because of the relatively low amplitude of the grouped displacement of atoms. Finally the temperature inside the box decreases progressively under the influence of the thermostat applied to atoms externally placed at the box boundaries since the system is completely relaxed after a few tens of ps.

Both first stages of the cascades, the ballistic one and the thermal one are shown in Fig. 1(b) and (c). In Fig. 1(d), the stable configuration is given after cooling and relaxation of the simulation box. In this latter figure, it appears that some octahedral interstitial sites along the <1 1 0> direction have been filled.

Fig. 2 shows the distance distributions of U (a) and O (b) atoms displaced over distances smaller than 1.6 nm after relaxation at 700 K, averaged on nine simulations. These distributions extend up to 9 nm but only 10 atoms have been displaced over 1.6 nm in average. The distributions of atoms after the displacement cascade (continuous lines) and the distribution of atoms due to thermal vibrations at 700 K only (dashed lines) are indicated in Fig. 2. This figure reveals several interesting features. Firstly, if atoms have covered distances inferior to ~0.15 nm, then they have not been moved out of their original lattice site. Secondly, it is clear from Fig. 2 that a vast majority of atoms (in fact more than 70% of all displaced atoms) cover distances less than one cell parameter (see also [13]). Finally, following the cascade event, displaced atoms occupy one of two possible crystallographic sites: an original lattice site or for a smaller proportion of displaced atoms interstitial octahedral sites. This is quite obvious from the U atom distribution, but less so regarding the O atom distribution. It was however checked by averaging atoms position upon time to remove the thermal spreading from the O displacement distribution.

3.2. Kinchin–Pease type modelling

A model based on a very simplified Kinchin–Pease (KP) [14] approach was developed in order to evaluate the energy density and distribution functions of the displaced atoms in the case of a diatomic material (here, U and O) and when the displacement thresholds are not necessarily small compared to the energy of the moving atoms. The strong assumption of this model is that the energy distribution of both moving particles generated by a collision is a couple of Dirac delta functions at the average energy of the particles after the collision (instead of being uniform between 0 and the energy of the incident particle as in the classical KP model). The energy ratio between the energy E_1 of the incident particle and that (E_2) of one of the particles after the collision is thus given by Eq. (1):

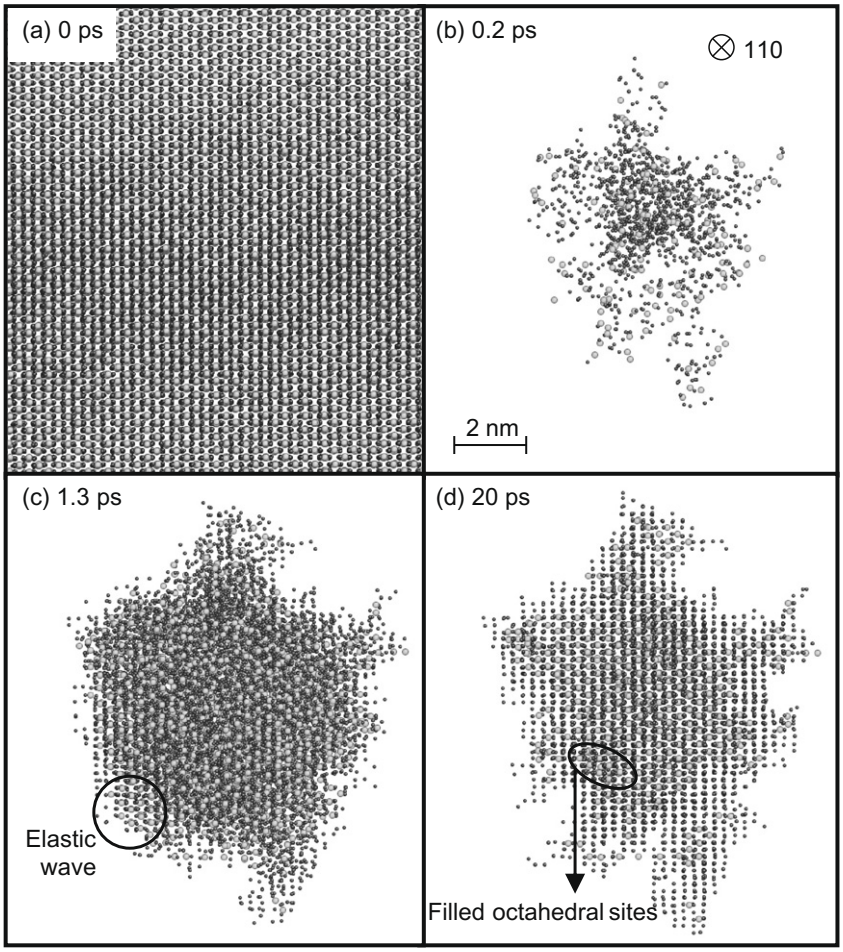

Fig. 1. Projections along the <1 1 0> direction of all atoms inside the initial simulation box (a) and of all displaced atoms which have covered more than 0.2 nm during the ballistic stage (b), the thermal stage (c) and the relaxation stage (d) of a cascade initiated with a 10 keV uranium PKA at 700 K. Dark circles represent oxygen atoms and light ones uranium atoms.

$$\frac{E_2}{E_1} = \frac{2M_1M_2}{(M_1+M_2)^2}. \tag{1}$$

Starting from the initial energy of the beam (U atom) E_0, the initial energy density function $\Delta_0^{\mathrm{U}}(E)$ of U is defined by the Eq. (2):

$$\Delta_0^{\mathrm{U}}(E) = \delta(E - E_0), \tag{2}$$

where δ is the Dirac delta function. The energy densities of new displaced U and O atoms are successively calculated at each generation, P_k^{O} and P_k^{U}, where k is the generation number. These density functions are evaluated on the basis of the total densities Δ^{U} and Δ^{O} of displaced U and O. The Δ's and P's densities are therefore sums of Dirac functions as shown in Eq. (3), for instance:

$$\Delta_k^X = \sum_l a_{kl}^X \delta\left(E - E_{kl}^X\right), \tag{3}$$

X standing for U or O. The vector transfer function that transforms the vector distribution function $\left(\Delta_k^{\mathrm{U}}(E);\ \Delta_k^{\mathrm{O}}(H)\right)$ of the kth generation in that of the $k+1$th is noted φ. This function is linear and defined according to Eq. (4):

$$\begin{pmatrix} \Delta_{k+1}^{\mathrm{U}}(E) \\ \Delta_{k+1}^{\mathrm{O}}(H) \end{pmatrix} = \varphi \begin{pmatrix} \Delta_k^{\mathrm{U}}(E) \\ \Delta_k^{\mathrm{O}}(H) \end{pmatrix} = \begin{pmatrix} \sum_l a_{kl}^{\mathrm{U}}\, \varphi_{\mathrm{UU}}\left[\delta\left(E - E_{kl}^{\mathrm{U}}\right)\right] + \sum_l a_{kl}^{\mathrm{O}}\, \varphi_{\mathrm{OU}}\left[\delta\left(E - E_{kl}^{\mathrm{O}}\right)\right] \\ \sum_l a_{kl}^{\mathrm{U}}\, \varphi_{\mathrm{UO}}\left[\delta\left(H - E_{kl}^{\mathrm{U}}\right)\right] + \sum_l a_{kl}^{\mathrm{O}}\, \varphi_{\mathrm{OO}}\left[\delta\left(H - E_{kl}^{\mathrm{O}}\right)\right] \end{pmatrix}, \tag{4}$$

φ can be decomposed in :

$$\begin{cases} \varphi_{\mathrm{UU}}(\delta_E) = 2p^{\mathrm{U}}\delta_{\alpha(E-Ed\mathrm{U})} + p^{\mathrm{O}}\delta_{\beta(E-Ed\mathrm{O})}, \\ \varphi_{\mathrm{OO}}(\delta_H) = 2p^{\mathrm{O}}\delta_{\alpha(H-Ed\mathrm{O})} + p^{\mathrm{U}}\delta_{\beta(H-Ed\mathrm{U})}, \\ \varphi_{\mathrm{UO}}(\delta_E) = p^{\mathrm{O}}\delta_{(1-\beta)(E-Ed\mathrm{O})}, \\ \varphi_{\mathrm{OU}}(\delta_H) = p^{\mathrm{U}}\delta_{(1-\beta)(H-Ed\mathrm{U})}. \end{cases} \tag{4.1}$$

The probability of any atom to knock an U atom is p^{U} regardless to the knocking atom (U or O), and symmetrically for p^{O}. These probabilities are roughly proportional to atomic fraction of each atom so that $p^{\mathrm{U}} = 1/3$ and $p^{\mathrm{O}} = 2/3$, as the radius of both atoms are close. Indeed an analysis of density of charges cartographies obtained from electronic structure calculations allows to roughly estimate Bader ionic radii of uranium and oxygen, respectively equal to 132 pm and 112 pm. α and β mean energy transfer coefficients calculated classically from the masses of atoms $\alpha = \frac{1}{2}$ is related to the O–O and U–U collisions, $\beta = \frac{2M_{\mathrm{U}}M_{\mathrm{O}}}{(M_{\mathrm{U}}+M_{\mathrm{O}})^2} = 0.88$ being to the U–O and O–U collisions. M_{U} and M_{O} stand for the respective atomic masses. Ed^{U} and Ed^{O} are the displacement thresholds respectively for U and O (here 40 and 20 eV according to [15,16]).

For instance, the first equation of Eq. (4) (concerning $\varphi_{\mathrm{UU}}(\delta_E)$), means that the energy distribution of the U atoms coming from a collision of an arbitrary number N of U atoms of energy E (distribution $N\delta_E$) with $p^{\mathrm{U}}N$ uranium atoms and $p^{\mathrm{O}}N$ oxygen atoms is $N\varphi_{\mathrm{UU}}(\delta_E)$: the $2Np^{\mathrm{U}}$ uranium atoms coming from the U–U collision have the energy $\alpha(E - Ed^{\mathrm{U}})$, the Np^{O} oxygen atoms (coming from the U–O collision) has the energy $\beta(E - Ed^{\mathrm{U}})$.

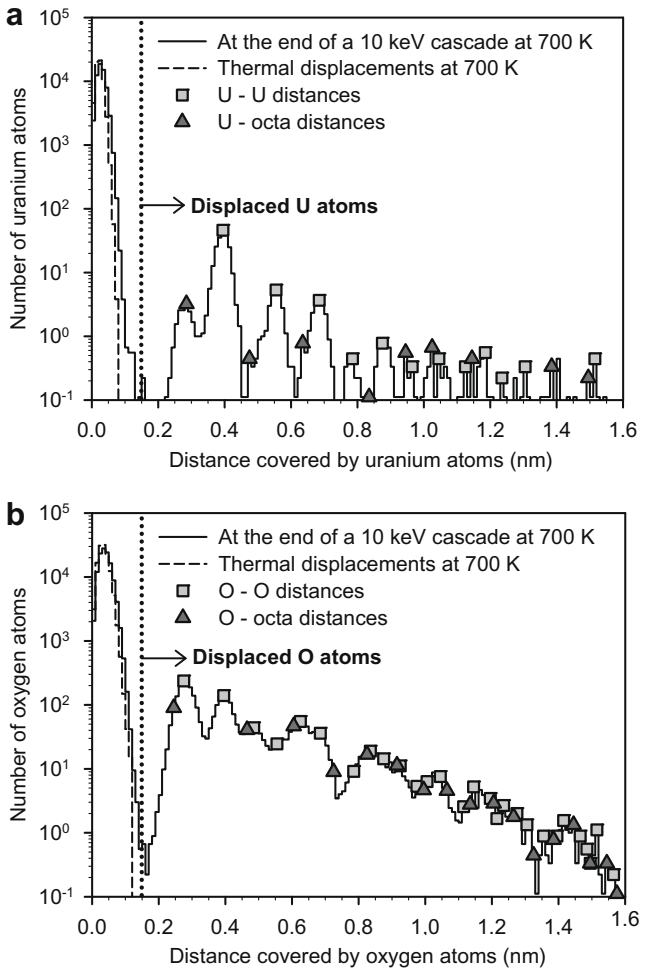

Fig. 2. Distribution of displacements up to 1.6 nm of uranium (a) and oxygen (b) atoms at 700 K which have been irradiation induced (continuous lines) or thermally induced (dashed lines). Each bar of histograms of 0.01 nm width shows the number of atoms averaged on nine calculations.

The densities of new displaced atoms can be evaluated the same way according to the Eq. (4.1) using the transfer function G:

$$\begin{pmatrix} P^{U}_{k+1}(E) \\ P^{O}_{k+1}(H) \end{pmatrix} = G \begin{pmatrix} \Delta^{U}_{k}(E) \\ \Delta^{O}_{k}(H) \end{pmatrix} = \begin{pmatrix} \sum_l a^{U}_{kl}\, G_{UU}\left[\delta\left(E - E^{U}_{kl}\right)\right] + \sum_l a^{O}_{kl}\, G_{OU}\left[\delta\left(E - E^{O}_{kl}\right)\right] \\ \sum_l a^{U}_{kl}\, G_{UO}\left[\delta\left(H - E^{U}_{kl}\right)\right] + \sum_l a^{O}_{kl}\, G_{OO}\left[\delta\left(H - E^{O}_{kl}\right)\right] \end{pmatrix}, \quad (5)$$

G can be decomposed in :
$$\begin{cases} G_{UU}(\delta_E) = p^{U}\delta_{\alpha E}, \\ G_{OO}(\delta_H) = p^{O}\delta_{\alpha H}, \\ G_{UO}(\delta_E) = p^{O}\delta_{(1-\beta)E}, \\ G_{OU}(\delta_H) = p^{U}\delta_{(1-\beta)H}. \end{cases}$$

Incremental application of φ and G is a simple (although, numerically inefficient) way of calculating the kth generation distribution. When the displacement thresholds are too small, the computation is too long and this simple technique is not suitable.

3.3. Energy distribution analysis using the Kinchin–Pease type model

The Kinchin–Pease type model described in the previous paragraph is used to interpret the energy cumulative distribution of displaced atoms in a cascade. The results of this simple model applied to a cascade initiated by a U atom of 10 keV are presented on Fig. 3. Each curve $N(E)$ represents the number N of displaced atoms whose energy was 'initially' (just after the collision) at least E. As expected, the simulated curves are quasi flat below the displacement threshold (here 40 eV for U and 20 eV for O [15,16]).

To compare this model with the MD calculations, the energy distributions of the displaced atoms of three 10 keV cascades were calculated on the basis of MD results (initial 10 keV U velocity, respectively, in the <100>, <110> and <19130> directions). Fig. 3 allows a comparison between the MD (at 20 ps) and KP type calculations. Fig. 4 displays oxygen energy distributions as calculated by MD. Each curve is related to a given time of the cascades (~0.1, 0.2, 1 and 20 ps), the first and second are before the fusion of the material, the third falls during the fusion and the last one after total relaxation (and re-solidification) of the box.

Fig. 3 reveals that at high energy both models for energy distributions are rather concordant. The differences occur mostly close to the beam energy, because at this energy level the number of displaced atoms of each generation is low, and the statistics is very poor (deviations from the average may be high). At lower energies:

- in the KP type model, the number of displaced O and U atoms saturates below 20 and 40 eV, respectively (according to displacement thresholds of the model).
- this number grows as time goes in the MD model and saturates around 1 eV.

From the Fig. 4, the time evolution of the distribution maximum can be interpreted in two ways:

- The cascade develops progressively and the first two snapshots (0.1 and 0.2 ps) were taken during this development, so that the energy maxima simply represent the energy of the current generation of moving atoms, far above the threshold, since the cascade is still running. The final distribution only occurs around 1 ps and is compatible with a ~1 eV displacement threshold. This value is much lower than commonly accepted for UO_2, which triggers a second interpretation.
- At the beginning of the cascade all the moving atoms have high energy and the distribution follows the KP type model irrespective to the negligible displacement threshold (which may be of a few tens of eV, as in solid materials). As far as the cascade progresses, displacement energy is deposited in the material whose temperature increases. For appropriate values of the displacement threshold, the material might melt before the energy of

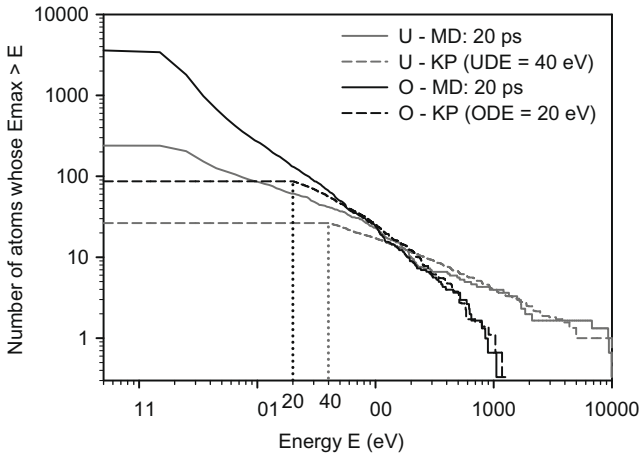

Fig. 3. Cumulative distributions of atoms $N(E)$ which have had a maximal energy superior to E, for cascades initiated at 10 keV estimated using a KP type model and from MD simulations at 700 K.

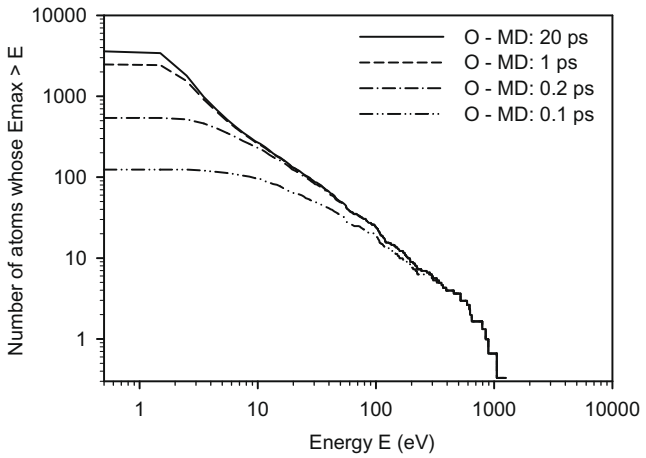

Fig. 4. Distributions of the number of oxygen atoms $N(E)$ which have had a maximal energy superior to E averaged on three cascades initiated at 10 keV and calculated by MD at 700 K; 0.1 ps and 0.2 ps refer to the ballistic stage of the cascade inside the solid UO_2 matrix, 1 ps to the cascade inside the partially molten material and 20 ps to the totally relaxed final state.

the moving particles reaches the threshold of the solid. The cascade then develops in a liquid whose apparent displacement threshold may be much lower than in a solid, around 1 eV as suggested by Fig. 3. The crude algorithm used here did not allow a simulation of a cascade with so small displacement threshold (the number of Dirac terms increases drastically). Nevertheless, one can suppose the general shape of the distribution would be maintained even at low energies (mainly cutoff of the distribution below the threshold).

To summarize, a Kinchin–Pease type model with very low displacement threshold (~1 eV) may account for the energy cumulative distribution function of the 10 keV cascades calculated by MD. This is compatible with the interpretation that the cascade, starting in a crystalline material, finally develops in a liquid, as stated for example in [17] on the basis of MD calculation of the density and temperature at the centre of the cascade in metals. It is likely that in such a liquid, the apparent displacement threshold is much lower than in the initial solid and that the created defects partially restore due to faster migration.

4. Uranium and oxygen radiation induced diffusion

4.1. Total square displacement values

The total square displacement R_X^2 is calculated from MD simulations according to Eq. (5), r_X being the distance between the initial and final positions of an atom:

$$R_X^2 = \sum_{\text{atoms}} (r_X > 0.15\ \text{nm})^2 \tag{6}$$

As it was previously mentioned in [13], the initial direction of the PKA was found to have no particular influence on calculation results. The total square displacement R_X^2 of atoms X in nm^2 was then averaged over all directions at each PKA energy and temperature.

4.2. Thermally activated diffusion

At 1400 K, oxygen diffusion occurs inside the simulation box. An NV″E″ calculation in the absence of a PKA was performed over a total time of 25 ps to estimate the R_X^2 corresponding to thermal diffusion. Less than a 100 oxygen atoms moved to different oxygen sites. Such a process is made possible by the fact that at this temperature, oxygen can occupy octahedral interstitial sites relatively frequently on the timescale of MD calculations. In an un-faulted UO_2 cell, two oxygen atoms **A** and **B** can exchange positions using the interstitial octahedral site as an intermediate position. Atom **A** initially moves to an interstitial position. **B** can then hop to the vacancy site thus made available by **A**, leaving another vacancy in its wake. **A** then hops to this site and exchange of positions between **A** and **B** has occurred.

In terms of total square displacement, this thermally induced mechanism was found to be small (less to 5 nm^2). At 1400 K, its contribution to the R_X^2 calculated from Eq. (5) is thus negligible so that the calculated R_X^2 remains the ballistic mixing contribution up to this temperature. Even if the performed calculation is too short to provide an accurate result, it has also been used to roughly estimate the thermally activated diffusion coefficient of oxygen at this temperature. This was estimated at around $10^{-13}\ m^2\ s^{-1}$, in quite good agreement with the extrapolation of Arrhenius curves for bulk UO_2 as deduced from MD simulations performed at higher temperatures using the same interatomic potentials [5,13]. Extrapolations at 1400 K of oxygen diffusion coefficients given in [18] between 1800 and 2600 K range between 4×10^{-15} and $4 \times 10^{-14}\ m^{-2}\ s^{-1}$. Our calculation furthermore satisfactorily corroborates the experimental results compiled by Belle [19] based on data obtained between 800 and 1600 K, for which the corresponding oxygen diffusion coefficient was estimated at between 10^{-14} and $10^{-12}\ m^{-2}\ s^{-1}$ at 1400 K.

4.3. Combined radiation and temperature effects

The number of displaced atoms and the values of R_X^2 are reported in Table 2. At a given PKA energy, they increase slightly with temperature. As suggested by Fig. 4, the majority of atoms are displaced during the second phase of the cascade event during which the molten phase appears. In this state, the energy required to displace atoms is conceivably comparable to their kinetic energy. In other words, on average, less energy is required from the cascade to displace an atom. Therefore, for a given cascade energy, more atoms are displaced at higher temperatures. Besides it was noticed that the contributions to the total square displacement of most atoms which displace over less than three times the cell parameter and of the few atoms which displace over at least this distance are comparable.

Fig. 5 reveals that R_X^2 is roughly proportional to the number of cascade overlaps (a) as it was previously shown in [13] and also to the energy of the PKA (b). The number of displaced atoms also increases proportionally to the PKA energy. It however appears not to be proportional to the number of cascade overlaps only due to the fact that an increasing number of atoms will be displaced several times during the successive cascades.

4.4. Application to the nuclear contribution of RID in-reactor and under long-term storage conditions

If the number of cascades F which occurs in a certain volume of fuel during a given time is known, it is then possible to estimate the diffusion coefficient $D_n(X)$ associated with the nuclear contribution to RID of element X using Einstein's equations [20] which lead to Eq. (6):

$$D_n(X) = \frac{1}{6 \times V_c \times d_X} F \times V_c \times R_X^2 = \frac{1}{6 \times d_X} F \cdot R_X^2 = K \cdot F, \tag{7}$$

where d_X is the volume density of element X, the factor 1/6 comes from the symmetry of the uranium dioxide fluorite structure [20] and V_c designates the volume occupied by displaced atoms following a cascade event. K is the proportionality constant between the

Table 2
Number of displaced atoms and values of total square displacement obtained from MD calculations. Data in italic are averaged over one to three MD simulations while other data are averaged over nine simulations. The cascade number refers to the total number of cascade which has been successively simulated within a same box.

Uranium PKA energy (keV)	Temperature (K)	Cascade number	Number of displaced atoms		Square displacement (nm^2)	
			U	O	U	O
80	300	1	*2400*	23 000	*600*	*8000*
10	1400	6	*2650 ± 165*	33 500 ± *1800*	*1385 ± 30*	25 125 ± *910*
10	1400	1	530 ± 107	8865 ± 352	195 ± 25	3000 ± 220
10	1100	1	462 ± 78	5546 ± 195	175 ± 36	1980 ± 150
10	700	14	*3376 ± 186*	20 760 ± *890*	*2325 ± 110*	18 800 ± *270*
10	700	1	292 ± 55	3746 ± 101	130 ± 18	1050 ± 130
5	700	1	119 ± 22	1680 ± 64	54 ± 6	390 ± 30
2	700	1	38 ± 10	564 ± 24	18 ± 3	105 ± 12
1	700	1	17 ± 4	243 ± 30	10 ± 2	37 ± 6

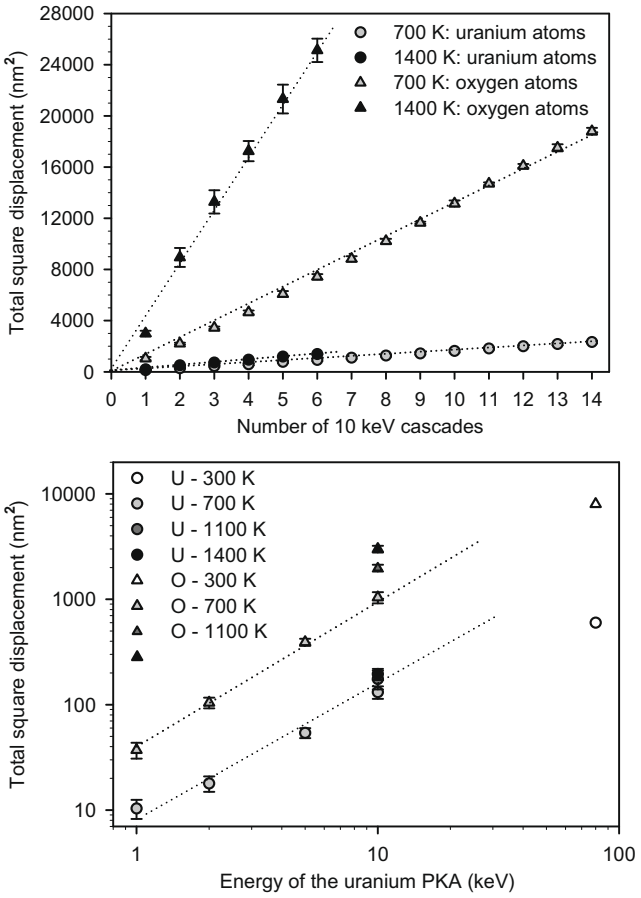

Fig. 5. Total square displacement of atoms R_X^2 versus the number of overlapped cascades (a) and versus the energy of the initial uranium PKA (b).

fission rate and the a thermal diffusion coefficient as defined in [2,3].

It is possible to extrapolate the values R_X^2 to higher energies as the total square displacement appears to be roughly proportional to the PKA energy. The nuclear contribution to RID can then be estimated considering the energy lost through nuclear interactions for a given particle. This energy loss is calculated by integrating the nuclear stopping power of the particle over the particle trajectory. For instance, a representative fission product such as a 100 MeV Xe nucleus loses 7 MeV through nuclear interactions in uranium dioxide (integration of its nuclear stopping power using TRIM 2003 [21]).

Finally it is also possible to roughly estimate the mean distance covered by U and O atoms in irradiation conditions for a time t using the classical Eq. (7):

$$\delta(X) \approx \sqrt{D_n(X) \times t}. \quad (8)$$

All calculation conditions and results relative to the application of Eqs. (6) and (7) to nuclear fuels under normal or long-term storage conditions are reported in Table 3. This table provides a reasonable estimate of the contribution to RID coefficients of ballistic mixing effects. These estimations are compared on Fig. 6 to some thermal diffusion coefficients and RID coefficients of O (a) and U (b) in UO_2 given in the literature [6,18,19], which have been eventually extrapolated.

As regards in-reactor data on Fig. 6(a), the estimated uranium diffusion coefficient which describes the ballistic mixing lies two to three orders of magnitude below that determined experimentally under comparable conditions [1–3]. It is therefore probable that nuclear collisions and the associated ballistic mixing do not provide an explanation for the observed movement of atoms under normal operating conditions. Electronic excitation which is not taken into account and/or defects enhanced diffusion could explain this difference. For oxygen, thermal diffusion coefficients range between 1×10^{-20} and 1×10^{-22} m^2 s^{-1} at 700 K and are therefore comparable to RID coefficients estimated here (Fig. 6(b)). At 1400 K

Table 3
Estimations of nuclear contributions to uranium and oxygen RID in in-pile and long-term storage conditions.

Environment	In-pile				Storage	
Cascade density F (m^{-3} s^{-1})	2×10^{19}				5×10^{15} (upper limit)	
Time t (a)	4				10 000	
Energy (keV)	7000				80	
Contribution to RID	Nuclear				Nuclear = total	
Temperature (K)	700		1400		700	
Element	U	O	U	O	U	O
A thermal coeff. K (m^5)	9×10^{-43}	3.4×10^{-42}	1.2×10^{-42}	10^{-41}	1.2×10^{-44}	5×10^{-44}
Diff. coeff. $D_n(X)$ (m^2 s^{-1})	1.7×10^{-23}	6.7×10^{-23}	2.4×10^{-23}	2.1×10^{-22}	6×10^{-29}	2.5×10^{-28}
Distance $\delta(X)$ (nm)	47	92	55	163	4	9
Displacements (dpa)	30		50		3	

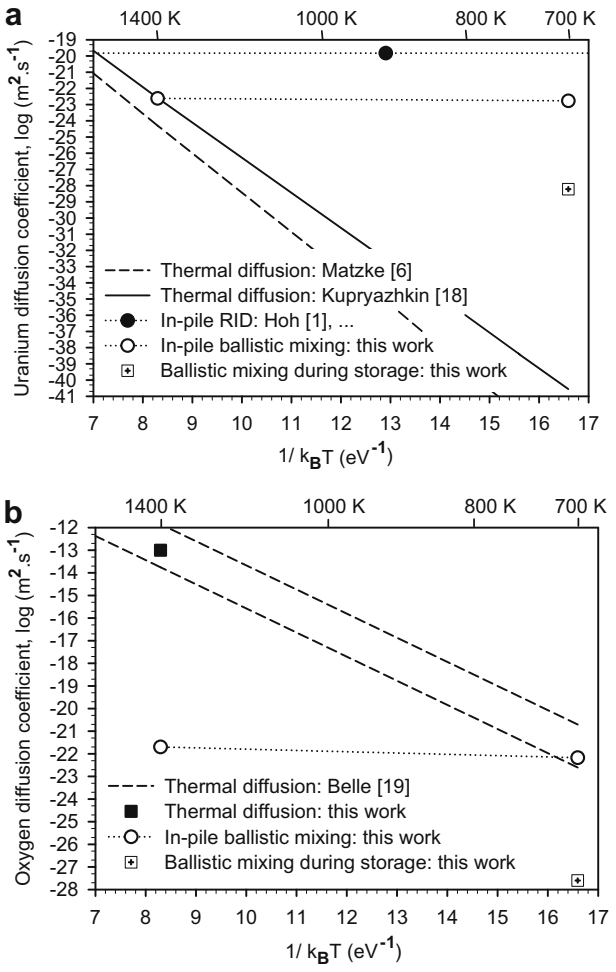

Fig. 6. Comparison of U (a) and O (b) thermal diffusion coefficients in UO_2 coming or extrapolated from the literature with the ballistic mixing contributions to the RID coefficient estimated in this work using MD in storage and in-pile conditions.

on the other hand, the ballistic contribution to the diffusion coefficient is negligible ($2 \times 10^{-22}\,m^2\,s^{-1}$ in comparison with the 1×10^{-14} and $10^{-12}\,m^2\,s^{-1}$ at 1400 K).

As regards long-term storage conditions, the values determined from this study are at least two to three orders of magnitude below those which are deemed relevant for spent nuclear fuels [22]. The same phenomena mentioned in the previous paragraph may be invoked to explain this difference. This is also worth noting that only recoil nuclei and not alpha particles have been assumed to contribute to the ballistic mixing, according to the results published in [12].

5. Conclusion

Molecular dynamics is a useful tool to study materials under irradiation and notably nuclear fuels. In this work, the phenomenology of the cascade was addressed: it was shown that the material melts at the end of the cascade, yielding a reduced threshold energy displacement. Radiation induced diffusion was investigated as well: the total square displacements were calculated for uranium PKA of energies up to 80 keV and at temperatures ranging between 300 and 1400 K. From these results the nuclear contribution to the RID was estimated for uranium and oxygen ions in in-reactor and long-term storage conditions. It is shown that the RID a thermal coefficient is well below those which are deemed relevant for spent nuclear fuels. This result probably applies to large size fission products such as iodine or xenon.

These first results relative to the ballistic mixing under irradiation can constitute a relevant dataset to feed models relative to the fuel behaviour under irradiation. Defect and defect aggregate formation consecutive to simulated irradiations will be published in a next paper.

Acknowledgements

This work was funded in part by the Basic Research branch (DSOE/RB) of the Nuclear Energy Division at CEA and the F-Bridge Project which is part of the European Union's Framework Programme 7.

All MD calculations were performed at the CCRT, the computing centre of Bruyères-Le-Chatel in France.

References

[1] A. Höh, Hj. Matzke, J. Nucl. Mater. 48 (1973) 157.
[2] J.A. Turnbull, C.A. Friskney, J.R. Findlay, F.A. Jonhson, A.J. Walter, J. Nucl. Mater. 107 (1982) 168.
[3] W.H. Hocking, R.A. Verrall, I.J. Muir, J. Nucl. Mater. 294 (2001) 45.
[4] L. Van Brutzel, M. Rarivomanantsoa, D. Ghaleb, J. Nucl. Mater. 354 (2006) 28.
[5] N.D. Morelon, D. Ghaleb, J.M. Delaye, L. Van Brutzel, Philos. Mag. 83 (2003) 1533.
[6] Hj. Matzke, J. Chemical Society, Faraday Trans. II 83 (1987) 1121.
[7] J.K. Fink, J. Nucl. Mater. 279 (2000) 1.
[8] J.E. Marin, P. Contamin, J. Nucl. Mater. 30 (1969) 16.
[9] Hj. Matzke, O.T. Sorensen (Eds.), Diffusion in Nonstoichiometric Oxides, Academic Press, New York, 1981.
[10] S. Nosé, Mol. Phys. 52 (1984) 255.
[11] J.M. Delaye, D. Ghaleb, Phys. Rev. B 135 (1998) 201.
[12] L. Van Brutzel, J.P. Crocombette, Ref. 0981-JJ01-01, in: Material Research Society Symposium Proceedings 981, MRS, Pittsburgh, 2007.
[13] L. Van Brutzel, M. Rarivomanantsoa, J. Nucl. Mater. 358 (2006) 209.
[14] G.H. Kinchin, R.S. Pease, Rep. Prog. Phys. 18 (1955) 1.
[15] J. Soullard, Contribution à l'étude des défauts de structure dans le dioxyde d'uranium, PhD thesis, Poitiers, France, 1976.
[16] J. Soullard, J. Nucl. Mater. 135 (1985) 190.
[17] H. Hsieh, T. Diaz de la Rubia, R.S. Averback, R. Benedek, Phys. Rev. B 40 (1989) 9986.
[18] A. Ya Kupryazhkin, A.N. Zhiganov, D.V. Risovany, K.A. Nekrassov, V.D. Risovany, V.N. Golovanov, J. Nucl. Mater. 372 (2&3) (2008) 233.
[19] J. Belle, J. Nucl. Mater. 30 (1969) 3.
[20] J. Philibert, Atom Movement, Diffusion and Mass Transport in Solids, Les éditions de Physique, Les Ulis, France, 1991.
[21] F. Ziegler, Nucl. Instrum. and Meth. B 219&220 (2004) 1026.
[22] C. Ferry, P. Lovera, C. Poinssot, P. Garcia, J. Nucl. Mater. 346 (2005) 48.